Inorganic Nanovehicle for Potential Targeted Drug Delivery to Tumor Cells, Tumor Optical Imaging

Shiyong Yu, Xuechuan Gao, Huricha Baigude, Xiao Hai, Renfei Zhang, Xiaolong Gao, Beibei Shen, Zhao Li, Zhibing Tan, and Haiquan Su*

College of Chemistry & Chemical Engineering, Inner Mongolia University, Hohhot 010021, Inner Mongolia, China

S *Supporting Information*

ABSTRACT: In this work, an inorganic multifunctional nanovehicle was tailored as a carrier to deliver anticancer drug for tumor optical imaging and therapy. The nanovehicle could be used as a dually targeted drug nanovehicle by bonded magnetical (passive) and folic acid (active) targeting capabilities. In addition, it was developed using rhodamine 6G (R6G) as a fluorescence reagent, and an α-zirconium phosphate nanoplatform ($Zr(HPO_4)_2 \cdot H_2O$, abbreviated as α-ZrP) as the anticancer drug nanovehicle. The novel drug-release system was designed and fabricated by intercalation of α-ZrP with magnetic Fe_3O_4 nanoparticles and anticancer drug 5-fluorouracil (5-FU), followed by reacting with a folate acid−chitosan−rhodamine6G (FA-CHI-R6G) complex, and then α-ZrP intercalated with Fe_3O_4 nanoparticles and 5-fluorouracil (5-FU) was successfully encapsulated into chitosan (CHI). The resultant multifunctional drug delivery system was characterized by scanning electron microscopy, X-ray diffraction, energy-dispersive X-ray analysis, photoluminescence spectra, magnetometry, fluorescence microscopy imaging studies and other characterization methods. Simultaneously, the drug release in vitro on the obtained nanocomposites that exhibited a sustained release behavior was carried out in buffer solution at 37 °C, which demonstrated clearly that the nanocomposites shown a sustained release behavior. Meanwhile, cell culture experiments also indicated that the drug-release system had the potential to be used as an dually targeted drug nanovehicle into the tumor cells.

KEYWORDS: *fluorescence imaging, controlled drug release, multifunctional drug-delivery systems, α-ZrP nanoparticles*
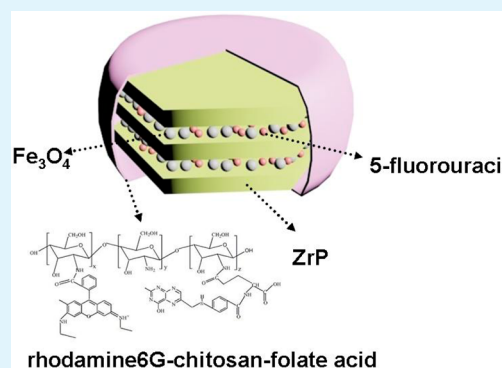
1. INTRODUCTION

It is widely known that many antitumor drugs have significant adverse effects due to the nonspecific uptake of drugs by normal cells.[1] Therefore, targeted drug delivery to tumor cells is crucial for the clinical therapy of tumors and it is imperative that the intellective targeted delivery of drugs system is developed to transmit medicinal materials to given tissue efficiently and achieve higher therapeutic efficacy.

One of the most promising approaches is to bond carriers with specific materials that have the capability to distinguish cancer cells. Folic acid (FA) that possesses high selectivity and binding affinity to the folate receptor that is expressed on many cancer cell surfaces has been used as a stable and effective target-specific ligand.[2,3] In recent decades, on the contrary, the folate receptor has been rarely found on other normal cell surfaces.[4] Thus, the conjugation of nanocarriers with folate could be bonded to tumor cells.[5−8]

Further, to enhance the therapeutic effects, the delivery system of drugs could be anchored to the site of the tumor. Consequently, an effective external magnetic field is strongly expected to achieve higher target selectivity by moving the drug carriers into the given tissues. To the best of our knowledge, magnetic nanoparticles (Fe_3O_4) with high saturation magnetization and narrow size distributions can have strong responsiveness to an applied magnetic field and have been widely employed for separation of biomolecular delivery of drugs, cancer diagnosis and treatment.[9−11] During the fabrication of the multifunctional drug carriers, magnetic iron oxide nanoparticles introduced should be coated with suited materials to ensure their stability and biocompability.

Using the expandable interlayer space of inorganic layered nanomaterials (ILN), we are able to encapsulate magnetic magnetite nanoparticles into these inorganic substrates to form hierarchical structured nanomaterials with diverse functionality. Moreover, layered materials have been certified to be superior drug carriers.[12−17] Among the most studied ILN are layered α-zirconium phosphates (α-ZrPs), which are inorganic layered ion exchange materials with interlayer spacing of 7.6 Å, solid-state ion conductivity, high thermal stability and which are known as carrier devices for incorporating substrates of any sizes from ions to macromolecules.[18−21]

However, it is difficult to directly modify the surface of α-ZrP nanoparticles, which has limited their applications in biomedical fields. To impart stability and allow functionalization, the surfaces of α-ZrP nanoparticles can be coated with chitosan (CHI), which is a useable natural biopolymer that has been

widely applied for drug delivery ascribable to its attractive properties, such as good biocompatibility, biological modification, security, biodegradability and distinctive chemical reactivities.[22,23] The peripheral hydroxyl and amine groups on the molecular chain of CHI can be modified with other functional groups. In addition, CHI does not induce immune rejection or allergic reactions and it has sticky properties that extend its holding to targeted matrix.[24−27]

Further, the fluorescent drug carrier with magnetic nanoparticles can be employed as one of the most widely used way to track drugs in living cells. Rhodamine 6G (R6G), which can be easily immobilized onto the chitosan, has the potential to be used as fluorescent probe.[28] Here we bring out the preparation of an intelligent drug delivery system for coincidental tumor-drug delivery and fluorescence imaging (Scheme 1). For this

Scheme 1. Schematic Diagram of Designing 5-FU/Fe$_3$O$_4$/α-ZrP@CHI-FA-R6G Nanocomposites
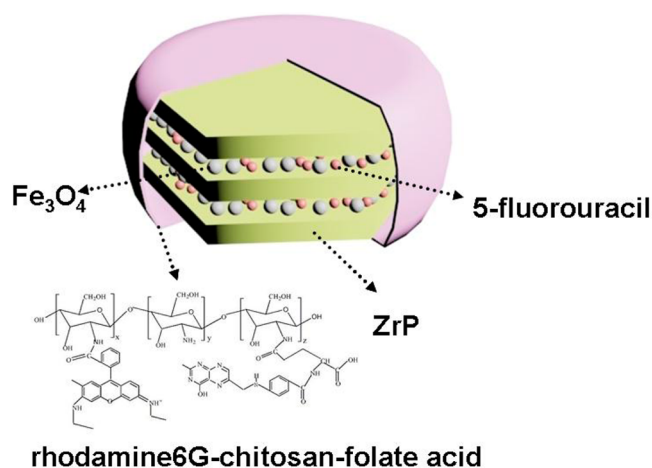
system, magnetic magnetite nanocrystals were intercalated into the α-ZrP interlayer after the preintercalation of C$_4$H$_9$NH$_2$ via the facile ultrasonic approach. Then the Fe$_3$O$_4$ nanoparticles modified α-ZrP was loaded with 5-FU as an anticancer drug and coated with CHI that was labeled with R6G molecules and FA molecules. The obtained drug delivery systems were designated as 5-FU/Fe$_3$O$_4$/α-ZrP@FA-CHI-R6G and were characterized via different techniques.

2. EXPERIMENTAL SECTION

2.1. Preparation of α-ZrP. The α-ZrP nanoparticles can be prepared with good control over the size and size distribution as modified from a previous report.[29] In a typical procedure, 41.5 mL of H$_3$PO$_4$ (85%) was added in 18.5 mL of deionized water with stirring. 6 g of ZrOCl$_2$·8H$_2$O was added into the suspension to produce a sol−gel system under continuous stirring. After that, the solution was hydrothermally treated for 24 h at 200 °C. After the hydrothermal reaction, the aggregates were washed twice with deionized water, and then vacuum-dried at 65 °C. Then they were dispersed into 100 mL of distilled water to form the α-ZrP suspension.

2.2. Preparation of Magnetic Fe$_3$O$_4$ Nanoparticles. Monodispersed Fe$_3$O$_4$ nanoparticles with uniform size distribution were achieved by the chemical coprecipitation method.[30] Briefly, 125 mL of NH$_3$·H$_2$O (0.04 M) was added into a 12.5 mL mixture of FeCl$_3$ and FeSO$_4$ (molar ratio was 2:1) under continuous stirring and nitrogen conditions. Then a black precipitate was formed under N$_2$ protection. After that, the product was washed three times with distilled water and dispersed into 100 mL of distilled water for further use.

2.3. Preparation of Fe$_3$O$_4$/α-ZrP Nanocomposites. 3 mL of α-ZrP suspension, 6 mL of Fe$_3$O$_4$ aqueous solution and 6 mL of butylamine were added into the flask, followed by sonication for 2 h at room temperature. Finally, the as-prepared particles were washed several times with distilled water.

2.4. Preparation of 5-FU/Fe$_3$O$_4$/α-ZrP Nanocomposites. Typically, a given amount of Fe$_3$O$_4$/α-ZrP was added in deionized water, forming a solution to which was added 0.1 g of 5-FU. After that, the mentioned above solution was stirred at room temperature for 2 d. The products were purified by further centrifuging and washed three times with ethanol.

2.5. Preparation of FA-CHI-R6G. A solution of EDC (N-(3-(dimethylamino)propyl)-N-ethylcarbodiimide hydrochloride) and folic acid in 50 mL of dimethyl sulfoxide (DMSO) (molar ratio was 2:1) was prepared. Then the mentioned above solution was stirred at room temperature for 30 min in the dark. The solution was then added to an acetic acid aqueous solution that contained CHI and R6G (molar ratio was 1:1), and the solution was stirred for 16 h. Then, the solution was adjusted to pH 9.0.

2.6. Preparation of 5-FU/Fe$_3$O$_4$/α-ZrP@ FA-CHI-R6G Drug Delivery System. The novel drug delivery systems were prepared as follows: a given amount of 5-FU/Fe$_3$O$_4$/α-ZrP nanocomposites were added in deionized water in the flask, to which 0.1 g FA-CHI-R6G compounds were added, then sonication for 40 min. After that, the mixture was left to react for 1d under extensive stirring in the dark at room temperature. Subsequentiy, 1 mL of methanal solution was added and reacted for 1 h. Then the suspension was washed and centrifuged with deionized water. The resulting solid sample, denoted as5-FU/Fe$_3$O$_4$/α-ZrP@ FA-CHI-R6G, was dried in a vacuum oven at 30 °C.

2.7. Loading Efficiency of 5-FU. The concentration of 5-FU was determined using a standard 5-FU concentration curve (Figure 12) that could be obtained via series of 5-FU solutions with different concentrations at the wavelength of 265 nm using the UV−vis spectrophotometer. The drug loading efficiency was calculated by the following equation: loading efficiency (%) = $(m_1 − m_2)/m$, where m_1 was the initial amount of 5-FU, m_2 was the amount of 5-FU presented in the washes and m was the total volume of system. As was expected, 49% of loading efficiency of 5-FU on 5-FU/Fe$_3$O$_4$/α-ZrP@ FA-CHI-R6G was achieved.

2.8. In Vitro Cytotoxicity Assays of Fe$_3$O$_4$/α-ZrP@CHI-FA-R6G Nanocomposites. In vitro cytotoxicities of the samples were assessed on A549 cells by the MTT method. A549 cells were sown into a cell culture plate and were subsequently incubated for 24 h. Different concentrations of nanocomposites (0, 6.25, 12.5, 25, 50, 100 and 200 μg/mL) were then added to the wells. After the previous nutrient solution was removed, 20 μL of MTT solution was added into each well, then incubated for another 4 h. The plate was monitored at the wavelength of 450 nm using a microplate reader after 150 μL of DMSO was added.

2.9. Interaction of Multifunctional Nanomaterials with HeLa Cells. The HeLa and HEK293 cells were cultured on glass chamber slides in RPMI 1640 media containing 1% penicillin/streptomycin and 10% fetal bovine serum. The HeLa cells and HEK293 cells were washed three times with PBS, blocked in PBS containing BSA (1%) at 4 °C for 20 min. The cells were then incubated with 5-FU/Fe$_3$O$_4$/α-ZrP@FA-CHI-R6G nanocomposites (concentration 0.2 mg/mL). Then the cells were washed three times with PBS, and then imaged on a laser scanning confocal microscope (OLYMPUS, IX81). Cell targeting was detected on a laser scanning confocal microscope under a 488 nm excitation wavelength.

2.10. In Vitro Drug Release Behaviors Experiments. Release behaviors in vitro of 5-FU from 5-FU/Fe$_3$O$_4$/α-ZrP@FA-CHI-R6G drug delivery system was monitored in PBS (pH = 7.4). In short, 0.1 g of the obtained nanocomposites was mixed with 2 mL of PBS solution and then the mixture was added into a dialysis bag that was laid into a 50 mL centrifuge tube with 10 mL of buffer at pH 7.4 and incubated at 37 °C. 2 mL of solution was withdrawn, and the amount of 5-FU released from the composites was examined at 265 nm by recording the UV absorbance of the solution.
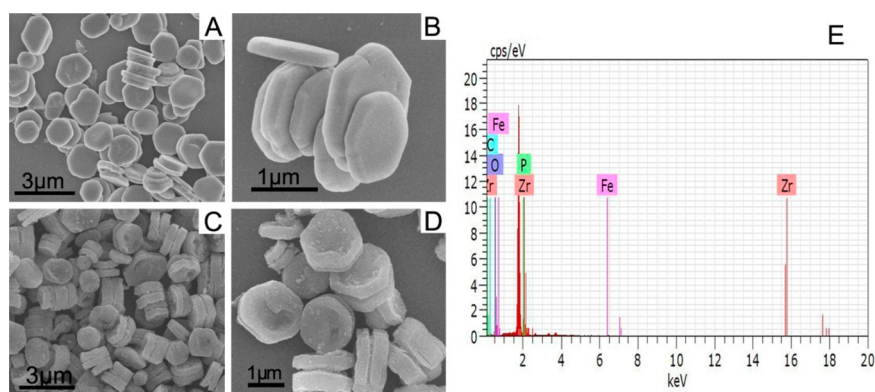
Figure 1. SEM images of α-ZrP at different magnifications (A,B); 5-FU/Fe$_3$O$_4$/α-ZrP@FA-CHI-R6G multifunctional nanomaterials at different magnifications (C,D); EDX imaging of the prepared nanocomposites (E).

3. RESULTS AND DISCUSSION

The structures and morphologies of α-ZrP and 5-FU/Fe$_3$O$_4$/α-ZrP@FA-CHI-R6G nanocomposites were obtained by scanning electron microscopy (SEM) images, as shown in Figure 1. The characteristic layered structure of α-ZrP could be observed in the SEM images of pure α-ZrP nanoparticles (see in Figure 1A,B). The 5-FU/Fe$_3$O$_4$/α-ZrP@FA-CHI-R6G nanocomposites shown observable existence of Fe$_3$O$_4$ nanoparticles between the interlayer of α-ZrP (Figure 1C). Furthermore, the surface morphologies of 5-FU/Fe$_3$O$_4$/α-ZrP@FA-CHI-R6G nanocomposites exhibited some harshness, which indicated the successful coating with FA-CHI-R6G, as shown in Figure 1D. Further, energy-dispersive X-ray (EDX) analysis was used to explain the elements contained in the 5-FU/Fe$_3$O$_4$/α-ZrP@FA-CHI-R6G drug-delivery system. The EDX results are presented in Figure 1E, which demonstrates that the C, P, Zr, O and Fe elements are integrated into the system.

Additionally, EDX elemental mapping in Figure 2 exhibits that Zr elements was distributed throughout the 5-FU/Fe$_3$O$_4$/α-ZrP@CHI-FA-R6G nanocomposites, while Fe existed in the interlayer of the nanocomposites and C was distributed on the nanocomposites randomly, which confirmed that 5-FU/Fe$_3$O$_4$/α-ZrP@CHI-FA-R6G nanocomposites were fabricated successfully.
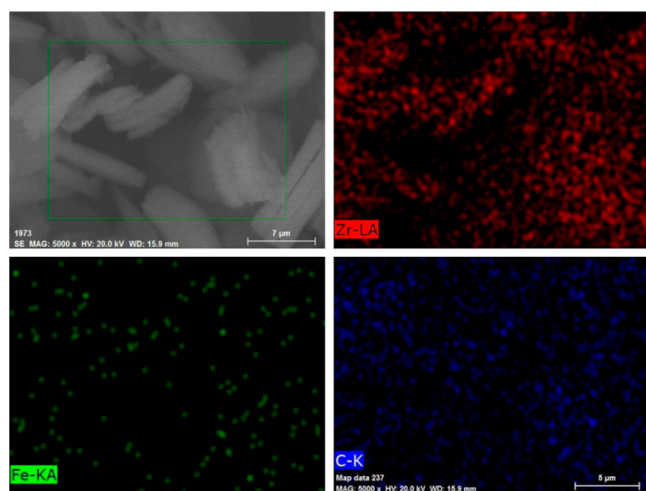

Figure 2. EDX elemental maps of the distribution of Fe, Zr and C elements in 5-FU/Fe$_3$O$_4$/α-ZrP@CHI-FA-R6G multifunctional nanosystem.

The X-ray diffraction (XRD) was employed to evaluate phase purity and crystal structures of the obtained nanocomposites. The XRD patterns of the obtained α-ZrP, Fe$_3$O$_4$/α-ZrP and 5-FU/Fe$_3$O$_4$/α-ZrP@FA-CHI-R6G samples are presented in Figures 3 and 4, respectively.
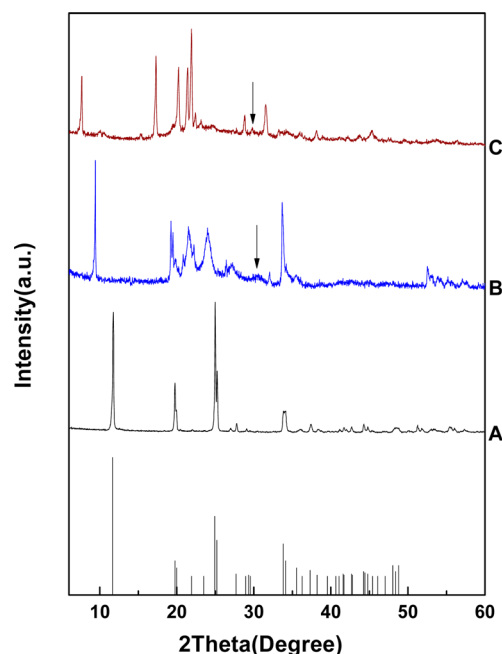
Figure 3. XRD patterns of α-ZrP nanoparticles (A), Fe$_3$O$_4$/α-ZrP nanocomposites (B) and 5-FU/Fe$_3$O$_4$/α-ZrP@FA-CHI-R6G multifunctional nanocomposites (C). The standard card of α-ZrP is given as a reference (PDF# 34-0127). The diffraction peaks noted with arrows ($\downarrow$) were indexed to Fe$_3$O$_4$.

In Figure 3A, the diffraction peaks matched the standard card (JCPDS No. 34-0127) well and no other impurity peaks were examined, indicating that α-ZrP well crystallized was achieved. A new peak assigned to Fe$_3$O$_4$ nanomaterials appeared at 30.1° in the XRD pattern (Figure 3B) of Fe$_3$O$_4$/α-ZrP, suggesting the successful insertion of Fe$_3$O$_4$ into the interlayer of α-ZrP. Further, the peak corresponded to Fe$_3$O$_4$ nanomaterials still existed in the XRD pattern of 5-FU/Fe$_3$O$_4$/α-ZrP@FA-CHI-R6G. However, the reflection peak intensity of Fe$_3$O$_4$ contained in the nanocomposites was relatively low, probably because the
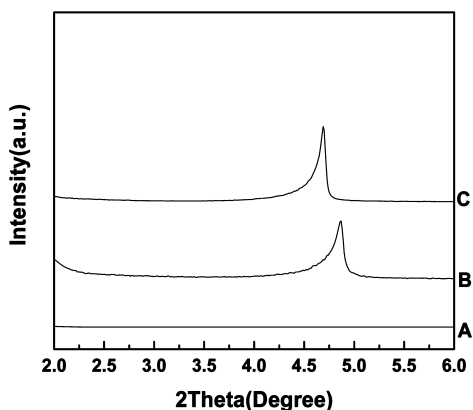
Figure 4. XRD patterns (2°–6°) of α-ZrP nanoparticles (A), Fe$_3$O$_4$/α-ZrP nanocomposites (B) and 5-FU/Fe$_3$O$_4$/α-ZrP@FA-CHI-R6G multifunctional nanomaterials (C).

crystallization degree of magnetic Fe$_3$O$_4$ nanomaterials in the composites was low.

The diffraction peak for α-ZrP was observed at 11.75°, corresponding to its basal spacing of 0.76 nm (Figure 3A). For the Fe$_3$O$_4$/α-ZrP composites, a diffraction peak was found at 4.86°, with the interlayer distance of 1.818 nm (Figure 4B). The increase of interlayer distance is 1.058 nm, which might be attributed to the intercalation of Fe$_3$O$_4$ and butylamine. For 5-FU/Fe$_3$O$_4$/α-ZrP@FA-CHI-R6G composites, a diffraction peak was found at 4.68°, corresponding to an interlayer distance of 1.888 nm (Figure 4C). The interlayer space was raised 0.007 nm from the Fe$_3$O$_4$/α-ZrP binary composites, indicating that 5-FU had been inserted into the interlayer of Fe$_3$O$_4$/α-ZrP. In addition, the XRD patterns of Fe$_3$O$_4$/α-ZrP and 5-FU/Fe$_3$O$_4$/α-ZrP@FA-CHI-R6G nanoparticles showed that all diffraction peaks corresponding to pure α-ZrP shifted to a lower 2θ value due to the extended interlayer distance.

FA-CHI-R6G conjugates could be prepared by chemically linking FA and R6G to CHI. The R6G, CHI, FA and CHI-FA-R6G conjugates were characterized by Fourier transform infrared (FTIR) spectroscopy. In the pure FA and R6G, the absorption bands that were appointed to the stretching vibrations of C=C in the backbone at 1608 and 1612 cm^{-1}, respectively (Figure 5A,C). The bands at or around 2921 and 2856 cm^{-1} corresponded to the characteristics of C—H vibrations, whereas the broad and intensive bands from 3500 to 3300 cm^{-1} belonged to the N—H and O—H vibrations, and the sharp peaks at 1384 cm^{-1} were associated with the CH$_3$ symmetrical deformation mode (Figure 5A,B,C,D). The stretching vibrations of C=O of carboxyl groups occurred at 1695 cm^{-1} in FA (Figure 5C). Meanwhile, the peak at 1124 cm^{-1} was assigned to the stretching bands of C—O—C of ester groups in R6G (Figure 5A). Compared with Figure 5A–C, the FTIR spectrum of CHI-FA-R6G conjugates (Figure 5D) contained the characteristic bands of CHI, R6G and FA. Moreover, the stretching vibrations of C=O of carboxyl groups at 1695 cm^{-1} disappeared and the stretching vibrations of N—H of amide groups at 1580 cm^{-1} emerged in the CHI-FA-R6G conjugate FTIR spectrum, suggesting a complete reaction between COOH in FA and NH$_2$ in CHI. In addition, the peaks due to C—O vibrations (1124 cm^{-1}) of C—O—C of R6G were shifted to 1088 cm^{-1}, confirming a strong interaction between R6G and CHI. Meanwhile, the results of
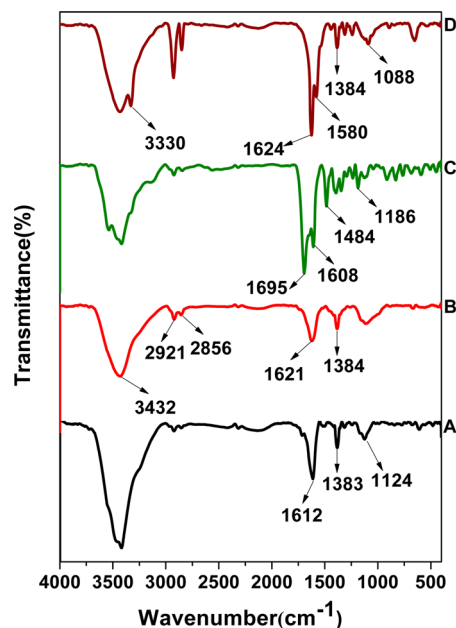

Figure 5. FTIR spectra of R6G (A), CHI (B), FA (C) and FA-CHI-R6G conjugates (D).

^{1}H NMR spectra also confirmed the covalent linkage of FA, CHI and R6G (Figure S1, Supporting Information).

Figure 6 represents the FTIR spectrum of 5-FU, Fe$_3$O$_4$/α-ZrP, 5-FU/Fe$_3$O$_4$/α-ZrP and 5-FU/Fe$_3$O$_4$/α-ZrP@FA-CHI-
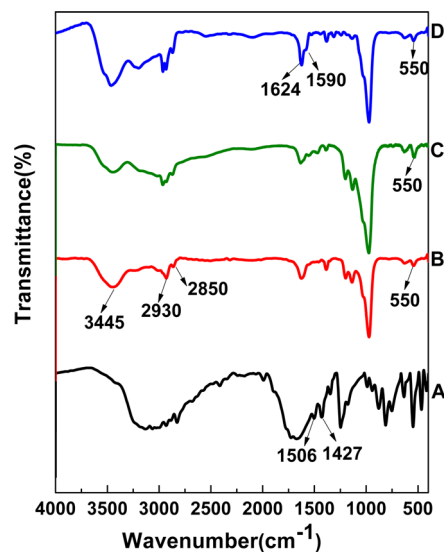
Figure 6. FTIR spectra of 5-FU (A), Fe$_3$O$_4$/α-ZrP nanocomposites (B), 5-FU/Fe$_3$O$_4$/α-ZrP nanocomposites (C) and 5-FU/Fe$_3$O$_4$/α-ZrP@folic acid−chitosan−rhodamine 6G conjugates (D).

R6G nanoparticles. The peaks at 1506 and 1427 cm^{-1} came from symmetric stretching vibrations of C=O and wagging vibrations of N—H in 5-FU, respectively (Figure 6A). The broad and intensive band from 900 to 1300 cm^{-1} was assigned to the phosphate group C$_{3v}$ vibration absorption in α-ZrP, while the band at 550 cm^{-1} was attributed to O—Fe absorption, confirming the existence of Fe$_3$O$_4$ in α-ZrP. In addition, two sharp absorption peaks at 2930 and 2856 cm^{-1} corresponded to the vibrations of methylene (CH$_2$) groups in C$_4$H$_9$NH$_2$, which demonstrated that Fe$_3$O$_4$ nanoparticles were

inserted into the interlayer of α-ZrP (Figure 6B). Compared to Figure 6B, some additional absorption bands assigned to the typical characteristics of 5-FU were observed in Figure 6C, indicating that the loading of 5-FU to α-ZrP via adsorption. Moreover, the FTIR absorption spectrum of 5-FU/Fe$_3$O$_4$/α-ZrP@FA-CHI-R6G multifunctional nanomaterials displayed all the characteristic absorbance of 5-FU, Fe$_3$O$_4$, α-ZrP and FA-CHI-R6G in Figure 6D, which clearly demonstrated that the multifunctional nanomaterials were fabricated successfully.

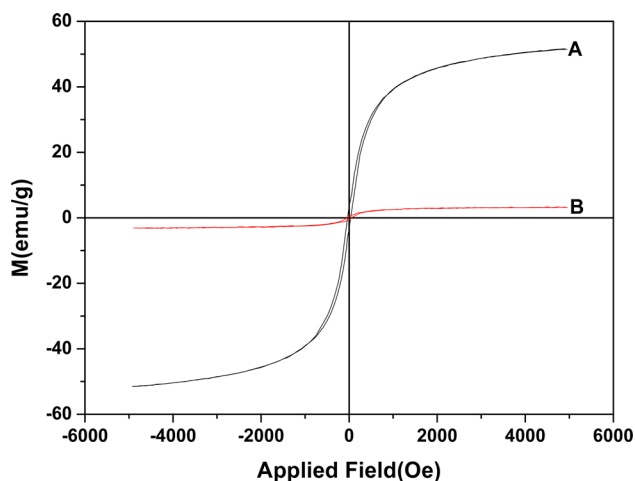Figure 7 displays the hysteresis loops (measured at 300 K) for Fe$_3$O$_4$ nanoparticles and 5-FU/Fe$_3$O$_4$/α-ZrP@CHI-FA-

Figure 7. Magnetic hysteresis loops of Fe$_3$O$_4$ nanoparticles (A) and 5-FU/Fe$_3$O$_4$/α-ZrP@CHI-FA-R6G multifunctional nanomaterials (B).

R6G multifunctional nanomaterials, which showed that both the original Fe$_3$O$_4$ nanoparticles and 5-FU/Fe$_3$O$_4$/α-ZrP@CHI-FA-R6G multifunctional nanomaterials displayed a magnetic behavior. The saturation magnetization value of 5-FU/Fe$_3$O$_4$/α-ZrP@CHI-FA-R6G multifunctional nanocomposites was 3.1 emu g^{-1} (Figure 7B), much lower than 51.5 emu g^{-1} of pure Fe$_3$O$_4$ (Figure 7A). This phenomenon was mainly attributed to the shielding effect of the ZrP or CHI multilayer and the relatively lower density of magnetic nanoparticles in the composites. Fortunately, this value could already fulfill the requirement of magnetic guiding, as found in Figure 8. Nanocomposites were dispersed uniformly in water to obtain
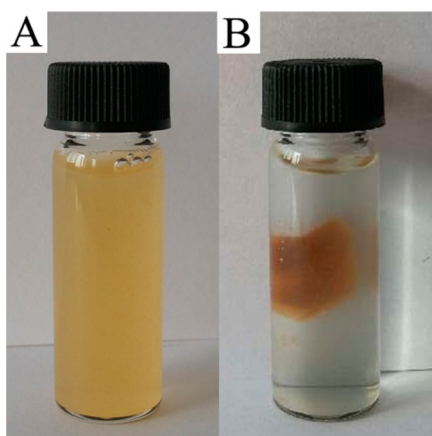

Figure 8. Photographs of 5-FU/Fe$_3$O$_4$/α-ZrP@CHI-FA-R6G nanocomposites without (A) and with the external magnetic field (B).

a brown dispersion before applying a magnet (Figure 8A). After a short time, the brown particles were drawn to the glass wall by applying an external magnetic field (Figure 8B).

Figure 9 shows the fluorescent properties of 5-FU/Fe$_3$O$_4$/α-ZrP@CHI-FA-R6G nanocomposites. Upon excitation at 404
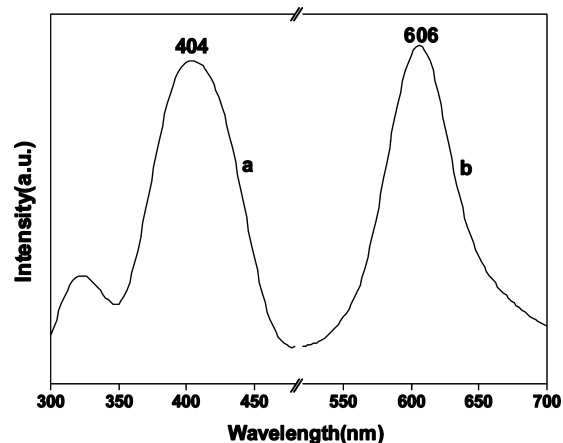

Figure 9. (a) Excitation (λ_{em} = 606 nm) and (b) emission spectra (λ_{ex} = 404 nm) of 5-FU/Fe$_3$O$_4$/α-ZrP@CHI-FA-R6G mutilfunctional nanocomposites.

nm, the obtained nanocomposites exhibited an intense emission peak at 606 nm, which suggested that the prepared nanocomposites were potentially effective and promising candidates for bioimaging.

The A549 cells were employed to measure the in vitro cytotoxicity of Fe$_3$O$_4$/α-ZrP@CHI-FA-R6G nanomaterials using the MTT method. Figure 10 shows the cell viabilities
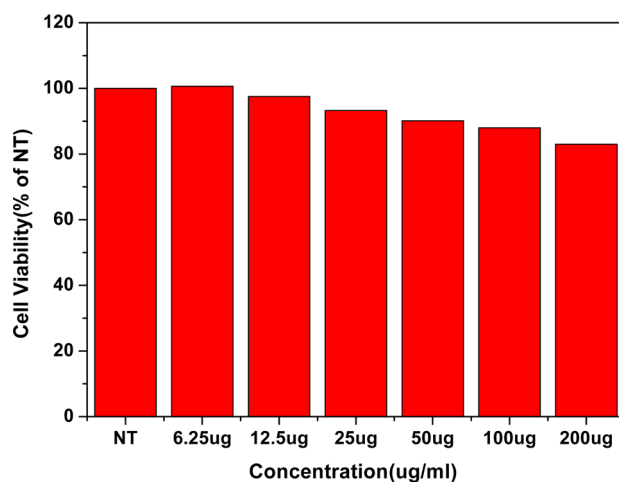

Figure 10. Cell viabilities of Fe$_3$O$_4$/α-ZrP@CHI-FA-R6G mutilfunctional nanocomposites to A549 cells measured by MTT.

against Fe$_3$O$_4$/α-ZrP@CHI-FA-R6G at different concentrations. It could be found that the nanomaterials had no obvious cytotoxic effects on A549 cells after 24 h of treatment with the samples at a concentration as high as 200 μg/mL, which indicated that the Fe$_3$O$_4$/α-ZrP@CHI-FA-R6G nanomaterials were biocompatible and could be potentially applied as targeted drug-delivery system.

The ability of 5-FU/Fe$_3$O$_4$/α-ZrP@CHI-FA-R6G nanocomposites to interact with FA positive HeLa cells and FA

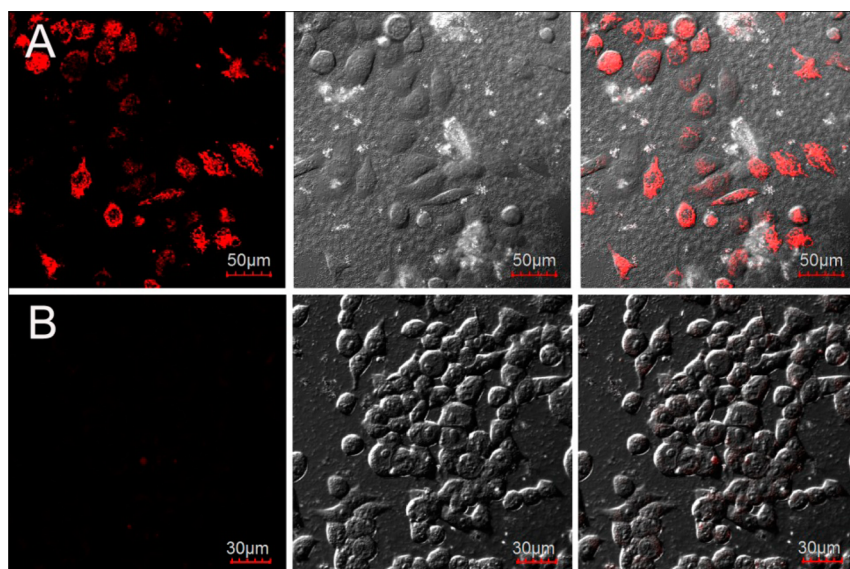**Figure 11.** Confocal laser scanning microscopy (CLSM) images of live HeLa cells (A) and HEK293 cells (B) after being incubated with 5-FU/Fe$_3$O$_4$/α-ZrP@CHI-FA-R6G multifunctional nanomaterials for 4 h. Left panel shows fluorescent images of dark field, the middle one represents images in bright field and the right one is an overlay of the left and middle panels.

negative HEK293 cells has been tested. Figure 11 shows CLSM of live HeLa cells and HEK293 cells incubated with 5-FU/Fe$_3$O$_4$/α-ZrP@CHI-FA-R6G multifunctional nanomaterials for 4 h. The red signal came from R6G in the obtained nanomaterials. It is clearly that 5-FU/Fe$_3$O$_4$/α-ZrP@CHI-FA-R6G nanomaterials could be taken on by the HeLa cells completely and displayed the strong luminescence signals while the HEK293 cells show little uptake of the nanomaterials, which confirmed the targeting capabilities of as-prepared drug delivery system.

A standard 5-FU concentration curve is shown in Figure 12. It is clearly that the absorbance was proportional to the amount
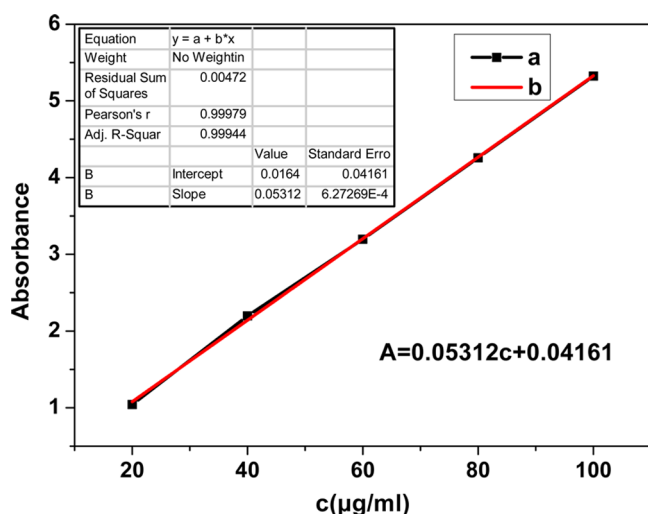
concentration of 5-FU released from the system could be obtained.

The cumulative drug release from 5-FU/Fe$_3$O$_4$/α-ZrP@CHI-FA-R6G multifunctional nanocomposites, expressed as the proportion of total drug released, is shown in Figure 13 as a

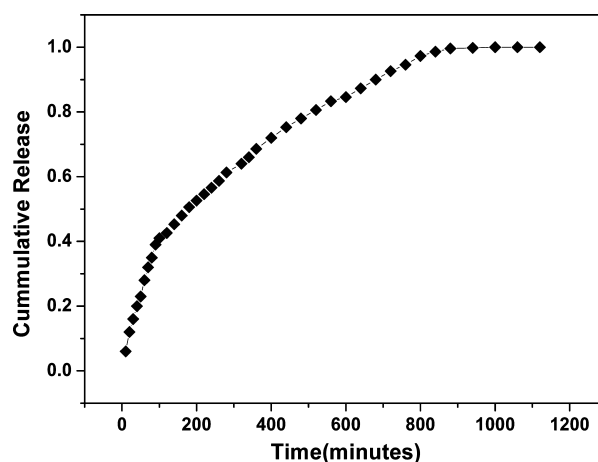**Figure 13.** Drug release profiles in PBS for 5-FU/Fe$_3$O$_4$/α-ZrP@CHI-FA-R6G multifunctional nanomaterials.

function of release time. Obviously, the curve presented mainly two stages: beginning rapid drug release period and subsequent slow release step. This initial rapid drug release might be induced by the quick release of 5-FU molecules absorpted on the surface of the nanocomposites. The other 5-FU molecules entrapped into the nanocomposites were released slower and incessantly by diffusion even after 1000 min. This result implied that the obtained drug delivery system was potential with a capability for controlled drug release.

4. CONCLUSION

The inorganic multifunctional nanovehicle (5-FU/Fe$_3$O$_4$/α-ZrP@CHI-FA-R6G) has been fabricated successfully for tumor optical imaging and therapy, which can be initially directed to

Figure 12. Absorbance of 5-FU in PBS as a function of concentration (a) and the calibration curve of a (b).

of 5-FU in the range from 20 to 100 μg/mL. Through the curve fitting, the standard equation of 5-FU could be figured out: $A = 0.05312c + 0.04161$, $R^2 = 0.99944$, where A was known as the absorbance, c was the concentration of 5-FU solution and R was the correlation coefficient. From the standard equation, the

the locations of cancer cells, and then recognized the cancer tissues by the biological affinity of FA. In addition, cell culture experiments proved the potential of the drug-release system as an effective dual targeting nanocarrier for the anticancer drug delivery into tumor cells and drug release in vitro on the obtained nanocomposites showed that the nanocomposites exhibited a sustained release behavior. These novel discoveries suggest that the new bioinorganic system can be an underlying material for use in bioimaging, drug targeting and bioseparation. Additionaly, this paper provides an efficacious method to explore inorganic layered materials as new targeted drug-delivery systems. The pursuit to apply such materials as drug-delivery systems is being carried out, and an extension of this method is underway in order to address broader biological applications.

■ ASSOCIATED CONTENT

ⓢ Supporting Information

Chemical structure of FA-CHI-R6G conjugate characterized by ^{1}H NMR. This material is available free of charge via the Internet at http://pubs.acs.org.

■ AUTHOR INFORMATION

Corresponding Author

*Prof. Haiquan Su. E-mail: Haiquansu@sina.com.

Notes

The authors declare no competing financial interest.

■ ACKNOWLEDGMENTS

■ REFERENCES

(1) Jang, S. H.; Guillaume, W. M.; Lu, D.; Au, J. L. Drug Delivery and Transport to Solid Tumors. *Pharm. Res.* **2003**, *20*, 1337−1350.

(2) Yang, S. J.; Lin, F. H.; Tsai, K. C.; Wei, M. F.; Tsai, H. M.; Wong, J. M.; Shieh, M. J. Folic Acid-Conjugated Chitosan Nanoparticles Enhanced Protoporphyrin IX Accumulation in Colorectal Cancer Cells. *Bioconjugate Chem.* **2010**, *21*, 679−689.

(3) Prabaharan, M.; Grailer, J. J.; Pilla, S.; Steeber, D. A.; Gong, S. Q. Folate-Conjugated Amphiphilic Hyperbranched Block Copolymers Based on Boltorn H40, Poly(L-lactide) and Poly(ethylene glycol) for Tumor-Targeted Drug Delivery. *Biomaterials* **2009**, *30*, 3009−3019.

(4) Mahato, R.; Tai, W. Y.; Cheng, K. Prodrugs for Improving Tumor Target Ability and Efficiency. *Adv. Drug Delivery Rev.* **2011**, *63*, 659−670.

(5) Stella, B.; Arpicco, S.; Peracchia, M.; Desmaele, T. D.; Hoebeke, J.; Renoir, M.; D'Angelo, J.; Cattel, L.; Couvreur, P. Design of Folic Acid-Conjugated Nanoparticles for Drug Targeting. *J. Pharm. Sci.* **2000**, *89*, 1452−1464.

(6) Bae, Y.; Jang, W. D.; Nishiyama, N.; Fukushima, S.; Kataoka, K. Multifunctional Polymeric Micelles with Folate-Mediated Cancer Cell Targeting and pH-Triggered Drug Releasing Properties for Active Intracellular Drug Delivery. *Mol. Biosyst.* **2005**, *1*, 242−250.

(7) Kamaly, N.; Kalber, T.; Thanou, M.; Bell, J. D.; Miller, A. D. Folate Receptor Targeted Bimodal Liposomes for Tumor Magnetic Resonance Imaging. *Bioconjugate Chem.* **2009**, *20*, 648−655.

(8) Liang, B.; He, M. L.; Xiao, Z. P. Synthesis and Characterization of Folate-PEG-Grafted-Hyperbranched-PEI for Tumor Targeted Gene Delivery. *Biochem. Biophys. Res. Commun.* **2008**, *36*, 874−880.

(9) Schladt, T. D.; Koll, K.; Prufer, S.; Bauer, H.; Natalio, F.; Dumele, O.; Raidoo, R.; Weber, S.; Wolfrum, U.; Schreiber, M. P.; Radsak, H.; Tremel, W. Multifunctional Magnetic MnO@SiO$_2$ Core/Shell Nano-

particles and Their Application for Optical and Magnetic Resonance Imaging. *J. Mater. Chem.* **2012**, *22*, 9253−9262.

(10) Mahmoudi, M.; Shokrgozar, M. A. Multifunctional Stable Fluorescent Magnetic Nanoparticles. *Chem. Commun.* **2012**, *48*, 3957−3959.

(11) Guo, M.; Yan, Y.; Zhang, H. K.; Yan, H. S.; Cao, Y. J.; Liu, K. L.; Wan, S. R.; Huang, J. S.; Yue, W. Magnetic and pH-Responsive Nanocarriers with Multilayer Core−Shell Architecture for Anticancer Drug Delivery. *J. Mater. Chem.* **2008**, *18*, 5104−5112.

(12) Zhu, Z. Y.; Zhang, F. Q.; Xie, Y. T.; Chen, Y. K.; Zheng, X. B. In Vitro Assessment of Antibacterial Activity and Cytotoxicity of Silver Contained Antibacterial HA Coating Material. *Mater. Sci. Forum.* **2009**, *620−622*, 307−310.

(13) Yu, S. Y.; Gao, X. C.; Jing, H.; Zhang, R. F.; Gao, X. L.; Su, H. Q. Fabrication and Characterization of Novel Magnetic/Luminescent Multifunctional Nanocomposites for Controlled Drug Release. *CrystEngComm* **2014**, *16*, 6645−6653.

(14) Tajima, T.; Suzuki, N.; Watanabe, Y.; Kanzaki, Y. Intercalation Compound of Diclofenac Sodium with Layered Inorganic Compounds as a New Drug Material. *Chem. Pharm. Bull.* **2005**, *53*, 1396−1401.

(15) Li, Y.; Li, H.; Wei, M.; Lu, J.; Jin, L. pH-Responsive Composite Based On Prednisone-Block Copolymer Micelle Intercalated Inorganic Layered Matrix: Structure and In Vitro Drug Release. *Chem. Eng. J.* **2009**, *151*, 359−366.

(16) Masarudin, M. J.; Yusoff, K.; Rahim, R. A.; Hussein, M. Z. Successful Transfer of Plasmid DNA into in Vitro Cells Transfected with an Inorganic Plasmid-Mg/Al-LDH Nanobiocomposite Material as a Vector for Gene Expression. *Nanotechnology* **2009**, *20*, 045602−045612.

(17) Xu, Z. P.; Walker, T. L.; Liu, K. L.; Cooper, H. M.; Lu, G. M.; Bartlett, P. F. Layered Double Hydroxide Nanoparticles as Cellular Delivery Vectors of Supercoiled Plasmid DNA. *Int. J. Nanomed.* **2007**, *2*, 163−174.

(18) Boo, W. J.; Sun, L. Y.; Liu, J.; Clearfield, A.; Sue, H. J. Effective Intercalation and Exfoliation of Nanoplatelets in Epoxy via Creation of Porous Pathways. *J. Phys. Chem. C* **2007**, *111*, 10377−10381.

(19) Kaschak, D. M.; Johnson, S. A.; Hooks, D. E.; Kim, H. N.; Ward, M. D.; Mallouk, T. E. Chemistry On The Edge: A Microscopic Analysis of The Intercalation Exfoliation, Edge Functionalization, and Monolayer Surface Tiling Reactions of α-Zirconium Phosphate. *J. Am. Chem. Soc.* **1998**, *120*, 10887−10894.

(20) Saxena, V.; Diaz, A.; Clearfield, A.; Batteasb, J. D.; Hussain, M. D. Zirconium Phosphate Nanoplatelets: A Biocompatible Nanomaterial for Drug Delivery to Cancer. *Nanoscale* **2013**, *5*, 2328−2336.

(21) Liu, L. M.; Zhang, H. T.; Shen, B.; He, W. J.; Liu, Y. G.; Lu, G. Y.; Zhu, J. J. PH-Induced Fabrication of DNA/Chitosan/α-ZrP Nanocomposite and DNA Release. *Nanotechnology* **2010**, *21*, 1051021−1051027.

(22) Jayakumar, R.; Menon, D.; Manzoor, K.; Nair, S. V.; Tamura, H. Biomedical Applications of Chitin and Chitosan based Nanomaterials - A Short Review. *Carbohydr. Polym.* **2010**, *82*, 227−232.

(23) Corato, R. D.; Bigall, N. C.; Ragusa, A.; Dorfs, D.; Genovese, A.; Marotta, R. Multifunctional Nanobeads Based on Quantum Dots and Magnetic Nanoparticles: Synthesis and Cancer Cell Targeting and Sorting. *ACS Nano* **2011**, *5*, 1109−1121.

(24) Thanou, M.; Verhoef, J. C.; Junginger, H. E. Oral Drug Absorption Enhancement by Chitosan and Its Derivatives. *Adv. Drug Delivery Rev.* **2001**, *52*, 117−126.

(25) Agnihotri, S. A.; Mallikarjuna, N. N.; Aminabhavi, T. M. Recent Advances on Chitosan based Micro- and Nanoparticles in Drug Delivery. *J. Controlled Release* **2004**, *100*, 5−28.

(26) Qi, L.; Xu, Z.; Jiang, X.; Hu, C.; Zou, X. Preparation and Antibacterial Activity of Chitosan Nanoparticles. *Carbohydr. Res.* **2004**, *339*, 2693−2700.

(27) Du, J.; Zhang, S.; Sun, R.; Zhang, L. F.; Xiong, C. D.; Peng, Y. X. Novel Polyelectrolyte Carboxymethyl Konjac Glucomannan-Chitosan Nanoparticles for Drug Delivery. II. Release of Albumin in Vitro. *J. Biomed. Mater. Res., Part B* **2005**, *72*, 299−304.

(28) Cho, H. S.; Dong, Z. Y.; Pauletti, G. M.; Zhang, J. M.; Xu, H.; Gu, H. C.; Wang, L. M.; Ewing, R. C.; Huth, C.; Wang, F.; Shi, D. L. Fluorescent, Magnetic Nanospheres for Drug Storage, Targeting, and Imaging: A Multifunctional Nanocarrier System for Cancer Diagnosis and Treatment. *ACS Nano* **2010**, *4*, 5398−404.

(29) Sun, L. Y.; Boo, W. J.; Sue, H. J.; Clearfield, A. Preparation of Alpha-Zirconium Phosphate Nanoplatelets with Wide Variations in Aspect Ratios. *New J. Chem.* **2007**, *31*, 39−43.

(30) Jiang, W. Q.; Yang, H. C.; Yang, S. Y.; Horng, H. E.; Hung, J. C.; Chen, Y. C. Preparation and Properties of Magnetic Nanoparticles with Narrow Size Distribution and Biocompatible. *J. Magn. Magn. Mater.* **2004**, *283*, 210−14.